Influence of Load, Surface Finish and Lubrication on Friction Coefficient of AISI 304 Stainless Steel

J. Dib, S. Hereñu, D. Alí, and N. Pellegri

The present work aims to evaluate the friction and wear behavior of a metastable stainless steel AISI 304L against steel AISI 52100 ball. Friction tests using the ''ball-on-disc'' technique at constant velocity (0.03 m/s) and different loads (6 N, 15 N) with and without lubricant (liquid vaseline) were carried out. Two surface finishing conditions were considered, leading to different mixture phases of preexisting austenite and martensite in the steel. One set of samples was polished to induce martensite (PO), and another set was tested in the as-received (AR) condition. Special emphasis was placed on correlating the friction and wear behavior with microstructural analysis performed by x-ray diffraction, optical, scanning electron and transmission electron microscopy. To complete the analysis, the microhardness profile was also performed for both PO and AR samples. The PO samples showed higher microhardness and greater amount of induced martensite and work hardening in the surface in comparison with AR samples. Independently of applied load and initial surface condition, two different stages on the friction behavior can be identified in dry tests. On the contrary, a stable behavior is observed in lubricated tests. Moreover, whereas in lubricated tests wear behavior is independent of surface finishing conditions and load, it shows a pronounced influence with load in dry tests.

1. Introduction

Austenitic stainless steels are widely used in the chemical, petrochemical and food processing industries due to their high resistance to corrosion and the excellent combination of strength, formability, ductility and toughness (Ref 1-3). During the forming processes of engineering parts, during the machining operation or in-service performance of austenitic stainless steel, its relative motion tends to induce friction and plastic deformation. Particularly, in low-alloy metastable austenitic stainless steel, plastic deformation can induce martensitic transformation (Ref 3, 4). Thus, as sliding continuously causes important plastic deformation on the contact surface, induced martensite is expected in this steel (Ref 5).

In the literature, there has been sustained activity towards studying the tribological properties of metastable austenite stainless steels under different sliding conditions (Ref 3, 5-12). After sliding wear tests, several authors found induced martensite on the worn surfaces of these steels (Ref 3, 6-10). It is important to emphasize that the amount of this induced martensite increases with the normal load, sliding distances and preexisting martensite (Ref 3, 6-9). Most of these researches were focused on studying independently friction coefficient (COF) behavior, wear mechanisms or microstructural features. In contrast, little work has been published correlating the

friction curves and wear behavior of AISI 304 steel with microstructure (Ref 5, 9-11). Wei et al. (Ref 5) found that when low loads are applied (5 N and 10 N), austenite γ is fully transformed to α' martensite. Due to its higher hardness and anti-adhesive tendency, COFs in these tests remain stable and lower wear rates are expected. On the contrary, testing with higher loads (30 N and 50 N) results in higher COFs and fluctuating friction curves due to the remnant more adhesive austenite on the worn surface, caused by the untransformed austenite continuously exposed as wear progresses. Under the same testing conditions, Hua et al. (Ref 11) reported that the wear mechanism of AISI 304 steel was adhesion and plowing. Using similar high loads, Wang et al. (Ref 9) reported the existence of two stages in friction behavior of AISI 304 steel. The initial stage exhibits high and unstable COF as a result of large amounts of soft and adhesive γ phase. As sliding continues, $\gamma \rightarrow \alpha'$ transformation evolves and a higher hardness is achieved, combined with a reduction in the austenite fraction. Thus, a stable lower COF stage takes place and wear resistance is improved. Again, adhesive and abrasive wear is observed. Chen et al. (Ref 10) dry-tested AISI 304 steel against itself at 30, 70 and 120 N, and they also found two COF stages. In this work, initial unstable stage is attributed to plastic deformation of surface asperities with subsequent adhesion. The highest wear rates are observed in this initial stage. As regards the stable COF stage, the effect is ascribed not only to martensitic transformation, but also to the agglomeration of small oxidized particles that works as a lubricant layer. Moreover, this layer prevents further wear loss and wear rates decrease.

As already mentioned, in metastable AISI 304 steels changes in microstructure during friction and wear behavior may occur. Then, friction curves versus time or distance contain great information about the state of the tribosystem and its tribodynamic processes. Currently, particularly in these materials, there is a need of a further comprehensive under-

J. Dib, S. Hereñu, D. Alí, and **N. Pellegri**, Instituto de Física Rosario, Bv. 27 de Febrero 210 Bis, 2000 Rosario, Santa Fe, Argentina. Contact e-mail: dib@ifir-conicet.gov.ar.

standing and control of friction to enhance tribological performance. Therefore, the aim of this work is to evaluate the developed features of the friction curves and wear mechanisms under different conditions of AISI 304L stainless steel and its correlation with microstructure. With this in view, two surface finishing conditions are considered leading to different mixtures of preexisting austenite and martensite in the steel. Moreover, two applied loads are evaluated with and without lubricant.

2. Material and Methodology

The material used in the present study is AISI 304L stainless steel, supplied in plate by Roberto Cordes SA, thickness 5 mm, with the following chemical composition: 0.023% C, 18.100% Cr, 1.190% Mn, 0.070% N, 8.000% Ni, 0.022% P, 0.002% S, 0.350% Si. The supplied surface finish was 2B, which means the following thermomechanical process: cold rolling followed by an annealing in oxidizing atmosphere, electrochemical pickling and final rolling with highly polished rolls (Ref 13). This condition will be referred as as-received (AR). The steel was wire-cut into disc specimens of diameter 25 mm. In order to achieve different percentages of preexisting martensite, some discs were ground finished by the successive use of SiC papers with 60, 120, 320, 400 and 600 grit sizes. This last surface finish will be referred in the present work as polished (PO). The grain size was obtained by the average grain intersection method.

Before the tribological tests, the material's microstructure was characterized by optical microscopy (OM) and transmission electron microscopy (TEM), using an Olympus PME3 optical microscope and an electronic transmission microscope TEM PHILIPS EM 300 operated at 100 kV. Moreover, the microhardness profile of the surface was measured. The Vickers microhardness tests were performed using a Shimadzu HMV-2 tester, with an applied load of 490.3 mN for a dwell time of 10 s. The values were obtained at different depths: 50, 100, 500 and 1000 μm. At each depth, five measurements were taken. The corresponding medium value and its standard deviation were calculated.

The roughness of the surface was also measured using a Mahr Pocket Surf PS1. The roughness filter cut off wavelength was set in accordance with DIN EN ISO 4288:2000 (Ref 14).

A ball-on-disc Wazau TMR60 tribometer was employed to perform wear tests. Certified grade 100 AISI 52100 alloy steel balls of 10 mm in diameter (67 HRC) were employed as the mating counterpart. According to ISO 3290-1:2014, surface roughness Ra parameter of these balls is 0.100 μm (Ref 15). Experiments were carried out on two different load values, two different surface conditions and with lubricant (L) and without lubricant (WL). Dry and lubricated sliding tribological tests were carried out at room temperature at a constant velocity 0.03 m/s for loads of 6 N and 15 N and sliding distance of 100 m. Vaseline was used as a lubricant in lubricated tests. Hertzian contact stress for this tribosystem was calculated with HertzWin 2.9.0 Hertz contact stress calculator (Ref 16), resulting in 510.1 MPa. Each test was repeated three times to ensure the reliability of the results. Prior and after tests, specimens were ultrasonically cleaned using acetone solution, dried and weighted by an analytical scale with 0.1 mg resolution. As the scatter in the resulting COF curves was small, for each tested condition the mean value of weight loss percentage was calculated.

To evaluate the existence of preexisting martensite on the surface and the induced martensite on the wear track of AR samples, x-ray diffraction (XRD) technique was used, using a Philips Pro X Pert diffractometer with Bragg–Brentano configuration using a wavelength of 1,54 A° (copper tube Cu-K$_\alpha$) with angle of incidence 3° (R3°). The measurement parameters were initial and final 2θ angles of 40° and 85°, respectively, unbound $\theta/2\theta$, step 0.05° and time per step of 2 s. Furthermore, the surface of AR and PO samples with non-grazing incidence was also analyzed (NR). X-ray quantitative phase analysis was performed by Rietveld refinement (Ref 17), using the Java-based software MAUD (Material Analysis Using Diffraction) version 2.79 released November 4, 2017 (Ref 18, 19). In all cases, the estimated error in each phase amount is ± 2 wt.%.

After tribological tests and to understand the wear mechanism, the wear tracks of AR samples were analyzed by a scanning electron microscope (SEM) LEITZ AMR1000 equipped with energy-dispersive x-ray spectroscopy (EDS).

3. Results and Discussion

3.1 Microstructural Characterization

Figure 1(a) and (b) shows the optical cross-sectional micrographs of AR and PO before the tribological tests. In both figures, equiaxed austenite grains are observed with an average size of 40 μm. In addition, deformation twins and martensite are detected. It is important to point up that the PO sample exhibits a greater amount of martensite.

In Fig. 2, XRD patterns corroborate the preceding observations. The diffraction peaks associated with austenitic (γ, fcc) planes (111), (200), (220) and (311) and martensitic (α', bcc) planes (110), (200) and (211) were analyzed.

The quantitative phase analysis obtained by MAUD of the preceding diffractograms at angle of incidence 3° (R3) and non-grazing incidence (NR) angles is presented in Fig. 3. With NR configuration, independently of the surface finish, a predominant austenite proportion in comparison with martensite one is measured. As regards R3 configurations, two important features of the surface should be remarked. First, it is evident that the martensite in the AR samples is restricted to a thin film layer of the surface. Secondly, it becomes apparent that the mechanical polishing procedure applied on PO samples induced an additional increase in the martensite proportion. Alves et al. (Ref 20) evaluated the influence of metallographic preparation on martensite formation in 304L steel. The samples were ground until grit sizes of 1200 and 2000 mesh and then polished with diamond of 6, 3, 1 and 0.25 μm. They found that the metallographic preparation did not induce phase transformation. Then, the existence of a remnant surface layer of martensite found in PO samples can be rationalized by the absence of additional grit sizes and diamond polishing procedure that could have eliminated all the preexisting martensite.

Figure 4 presents the dislocation features of AR and PO samples near the surface obtained by TEM. The AR samples were mainly characterized by planar dislocation structures (e.g., regularly planar dislocation arrays, dislocation pile ups close to grain boundaries and stacking faults) (Fig. 4a). In addition,
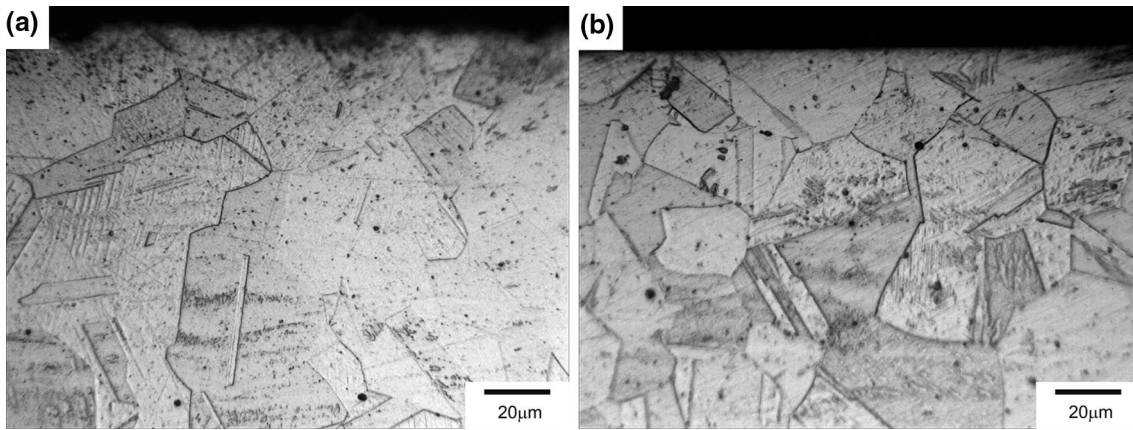
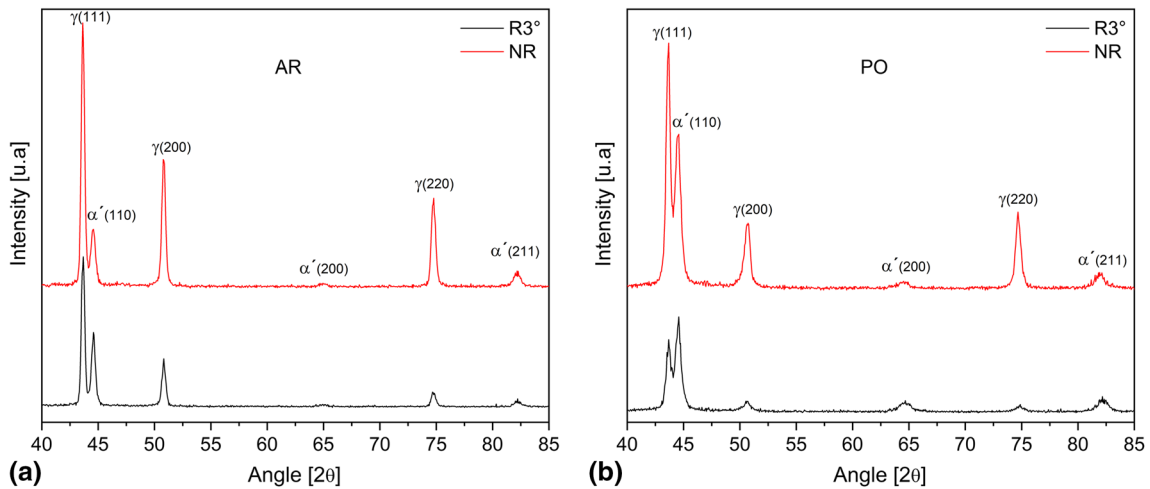**Fig. 1** Optical cross-sectional micrographs: (a) AR sample, (b) PO sample

Fig. 2 XRD patterns of the steel's surface. (a) AR sample, (b) PO sample
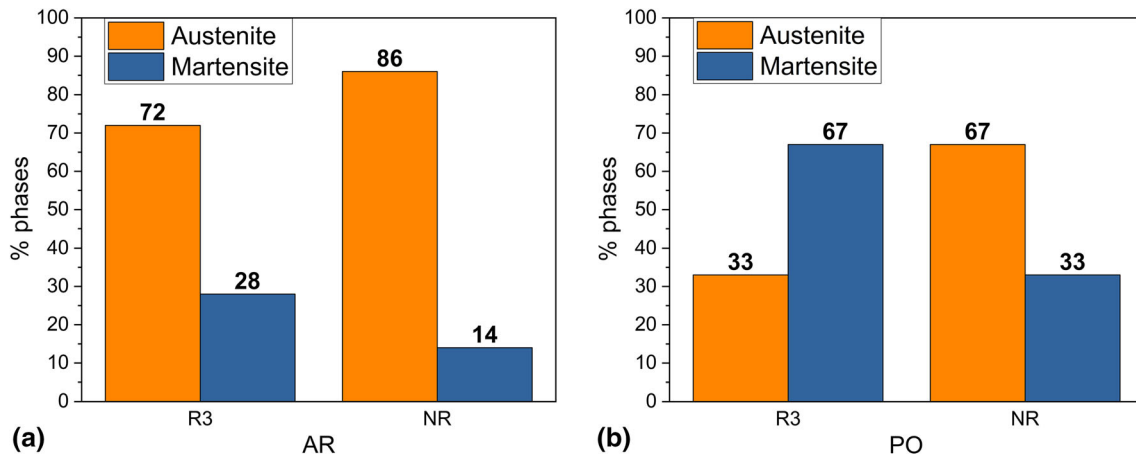

Fig. 3 Percentage of phases for samples: (a) AR, (b) PO

induced martensite was also observed in some grains (Fig. 4b). The dislocation arrangements of PO samples were similar to AR ones, except that the planar structures in the former condition were more tangled (i.e., within planar structures the dislocation density was higher and distributed homogeneously)

(Fig. 4c), and lathlike martensite α' was more often observed (Fig. 4d). Hence, TEM images of PO samples reveal an increase in work hardening and induced martensite in comparison with AR samples.
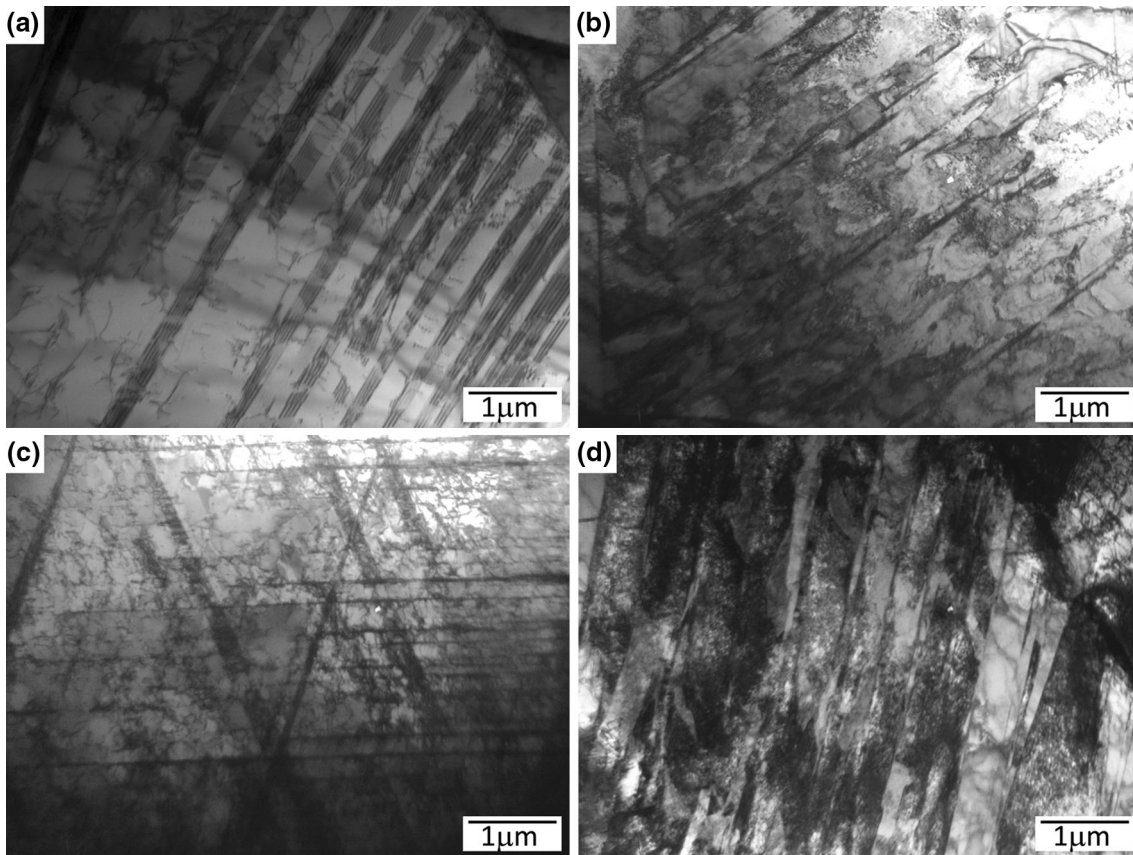
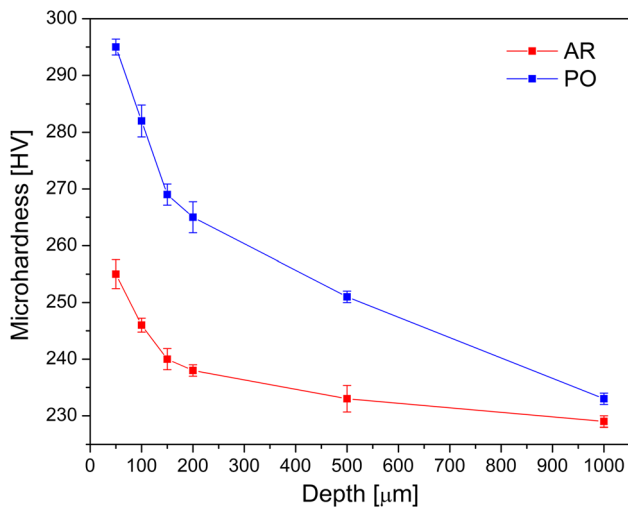**Fig. 4** TEM micrographs of AISI 304 steel. (a), (b) AR samples, (c), (d) PO samples

Fig. 5 Microhardness profile for AR and PO samples

3.2 Microhardness

Figure 5 shows microhardness profile for AR and PO samples.

It can be observed that as the depth increases, the microhardness decreases. This fact agrees with previous results where the martensite is mostly found on the surface (Fig. 3). In addition, the higher surface hardness in PO than in AR samples is consistent with the higher percentage of martensite and with

Table 1 Roughness parameters

Sample	Ra, μm	Rz, μm	Rt, μm
AR	0.72 ± 0.06	5.96 ± 0.42	7.97 ± 0.78
PO	0.034 ± 0.001	0.245 ± 0.034	0.311 ± 0.025

the work hardening-associated dislocation structure found in the former ones.

3.3 Surface Features

Table 1 presents the surface roughness parameters (Ra, Rz and Rt) for AR and PO samples. It can be seen from this table that PO sample presents lower roughness than the AR sample.

3.4 Tribological Properties

3.4.1 Influence of Surface Finish on Tribological Properties. Figure 6(a) shows the influence of surface finish on friction tests with and without lubricant at 6 N. Though the lubricant certainly decreases the friction coefficient (COF), evidence of the surface finish influence on friction behavior is observed neither with nor without lubricant. The above results are similar to those reported by Straffelini (Ref 21) in dry tests of Cu-8% Sn alloy against an AISI D2 tool steel with different roughness (Ra = 0.22 μm and Ra = 0.02 μm). In this work, an
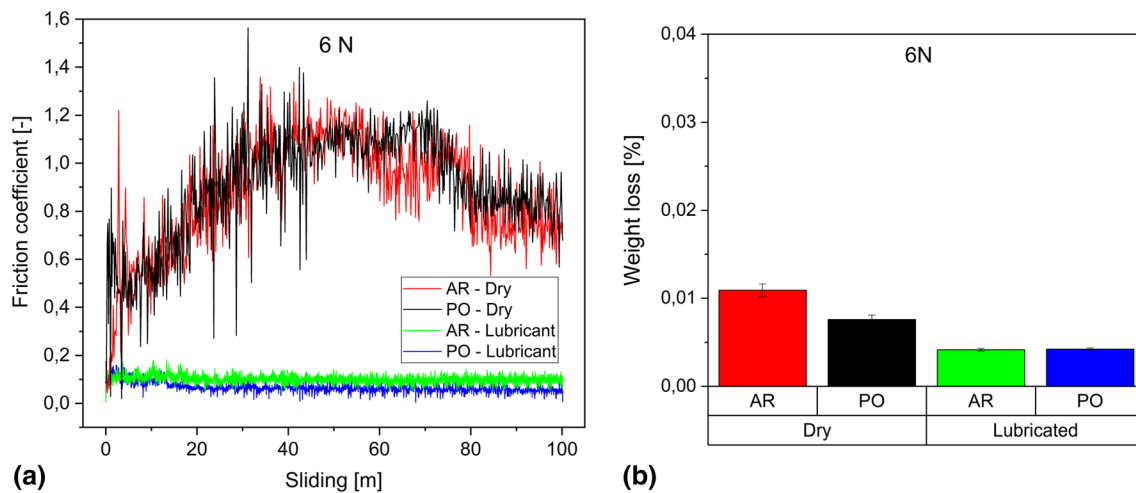
Fig. 6 Influence of surface finish on tribological properties with and without lubricant. (a) Friction coefficient, (b) weight loss percentages after friction tests

initial stage of COF (called ''running-in'') displays a slightly dependence on roughness. After the running-in, the same COF is achieved, due to the polishing of the mating surfaces. Thus, the same surface condition is reached. Furthermore, it was found that for tests carried out between pure aluminum and harder 080 M40 steel with different roughness, the COF is independent of the initial roughness values (Ref 22). It is well known that the initial surface features will quickly be erased if the contact pressures are high or if one or both contacting materials are relatively soft. In the present work, the same harder counterpart was used. Nevertheless, though AR surfaces are softer than PO ones (Fig. 5), which enhances the earlier worn off of the tallest peaks of the ground, its higher roughness (Table 1) counterbalances this effect. Thus, an equivalent COF for both surface fishing conditions (Fig. 6a) is achieved. Moreover, Fig. 6(b) shows that no appreciable influence of surface fishing conditions on weight loss percentages after friction tests is observed.

3.4.2 Influence of Applied Load on Tribological Properties. As no influence of surface finishing conditions on COF and wear was observed, only AR samples were selected for this study. Figure 7 shows the influence of applied load on tribological properties of tested AR samples. During sliding, several surface modifications may take place, i.e., material transfer, phase transformation, debris and oxide formation, that are relevant in friction and wear analysis. Figure 8 shows the XRD patterns for the different loads with and without lubricant in the worn track. The percentages of phases beneath the wear tracks under various friction tests are shown in Fig. 9. It is evident that friction tests induce a pronounced increase in the volume fraction of the transformed α' from the metastable γ (Fig. 3). With increasing loads, a significant increase in the percentage of martensite can be observed for dry samples, while there are no discernible changes in phase fraction for lubricated samples.

In order to understand the wear mechanisms involved in the studied tribological system, the resulting worn tracks were analyzed by SEM–EDS. It is known that the highest shear stress in the subsurface region in repeated compressive load conditions generates voids and cracks under the worn track. As the sliding progresses, these cracks propagate parallel to the

surface and coalesce, producing platelike debris (Ref 6, 7, 23, 24). Moreover, grooves associated with plowing are also found. The formation of these microgrooves could be caused by the higher hardness of the counterpart. For lubricated tests (Fig. 10a and 11a), delamination phenomena during the wear process are observed. After dry tests, worn tracks are characterized by cloudlike transfer lumps (Fig. 10b and 11b). These lumps are generated by material transfer when the surface is plastically deformed. Similar results were reported in (Ref 10). EDS spectrum of the AR material is shown in Fig. 12. Figure 13 and 14 exhibit the oxidized particles with the EDS spectrums found in the worn track in dry tests for 6 and 15 N, respectively.

It is known that when a harder material slides against a softer metal surface, the COF is dominated by two components: (a) adhesion and (b) plowing. Whereas the adhesive force is determined by the chemical composition of the surfaces, plowing depends on the surface conditions of the sliding surfaces (Ref 22, 23).

Figure 7(a) shows that no appreciable influence of load on friction behavior is detected at the beginning of the dry tests, particularly at the first 30 m slid. Later, the COF with 15 N load is more stable and exhibits lower values than with 6 N. Chen et al. (Ref 10) analyzed the different stages displayed by the COF in AISI 304 steel. In this context, they ascribed the initial unstable COF stage to the plastic deformation of asperities. Moreover, these authors attributed the subsequent lower and stable COF to the higher hardness of the induced α' martensite and work hardening, summed by the presence of oxidized particles. Their proposed mechanism to rationalize the COF stages is consistent with the results reported in this work. It is important to remark that though Chen et al. (Ref 10) obtained similar COF trends at higher loads, no detailed microstructural explanation in correlation with load is reported. In the present work, a higher COF is expected at 15 N since the amount of transfer lumps increase with load (Ref 25). This assumption is found comparing Fig. 10(b) with Fig. 11(b). Nevertheless, within this worn track a higher density of oxidized particles (Fig. 14a), and a higher percentage of martensite (Fig. 9a) are also observed. Oxidation effects can reduce friction due to the formation of a tribological layer that
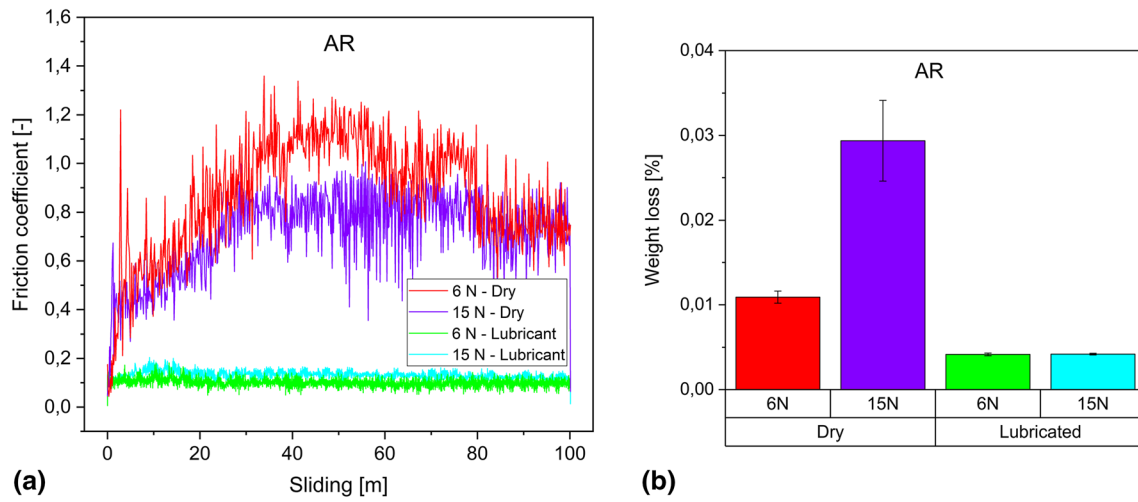
Fig. 7 Influence of applied load on tribological properties with and without lubricant. (a) Friction coefficient, (b) weight loss percentages after friction tests
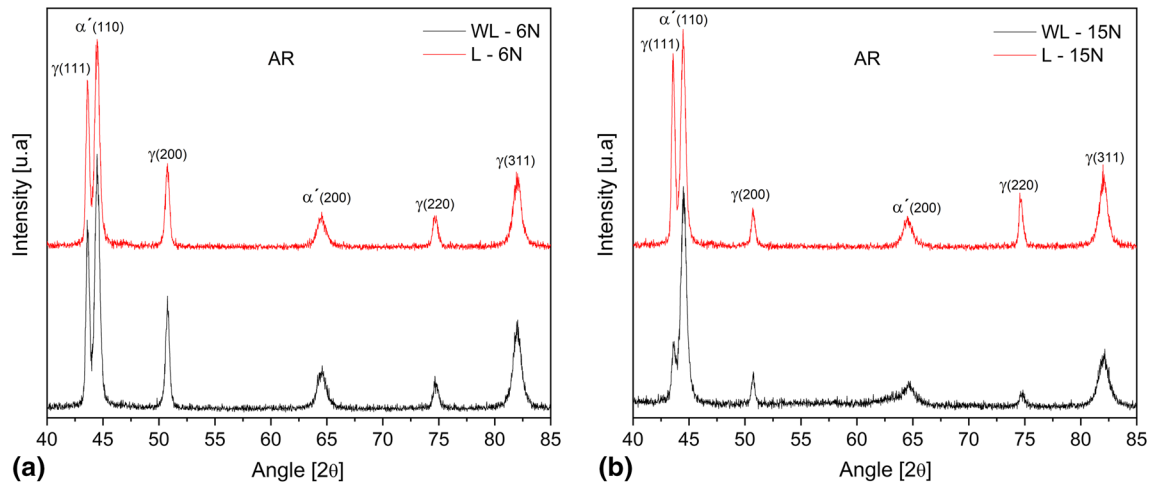

Fig. 8 Diffractograms obtained in the track, with and without lubricant. (a) load: 6 N, (b) load: 15 N
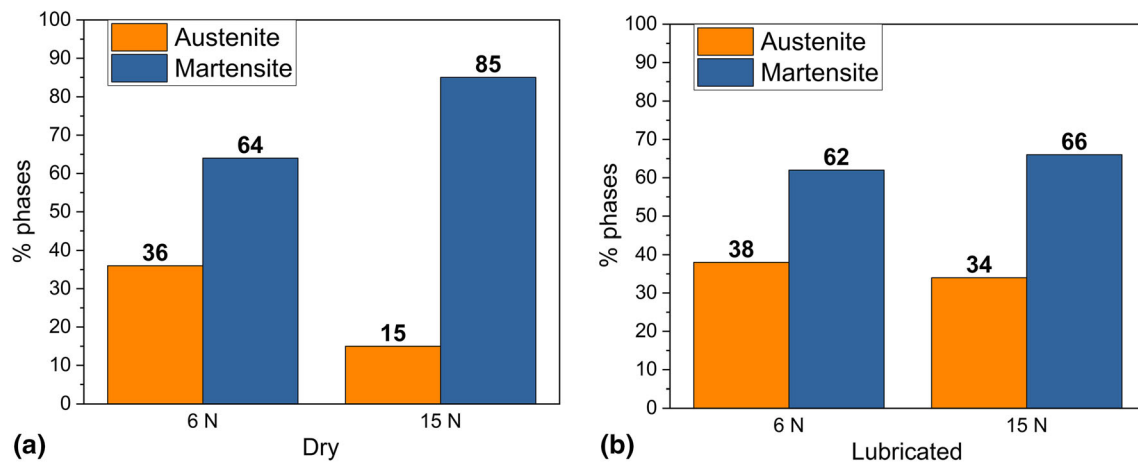

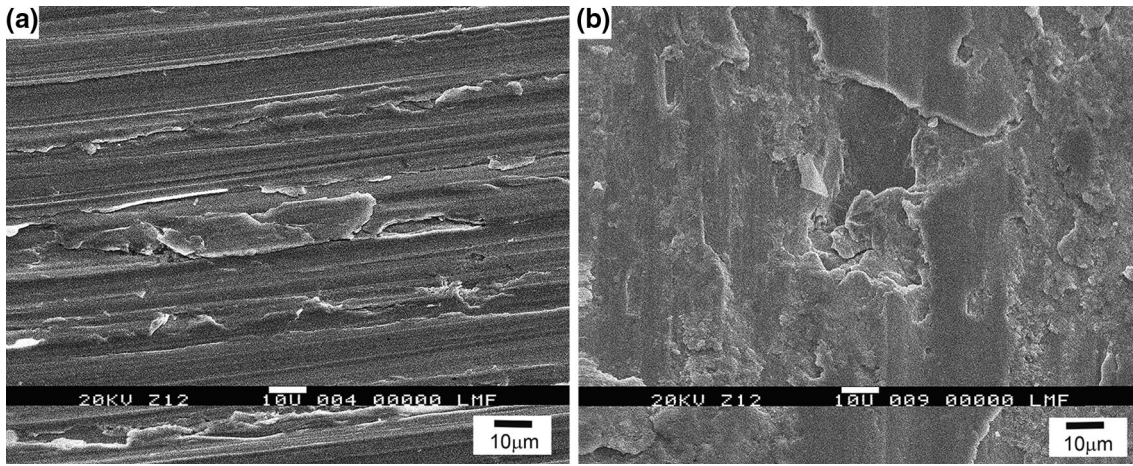**Fig. 9** Percentages of phases in the worn track. (a) Dry tests, (b) lubricated tests

Fig. 10 Worn tracks for 6 N. (a) With lubricant, (b) without lubricant
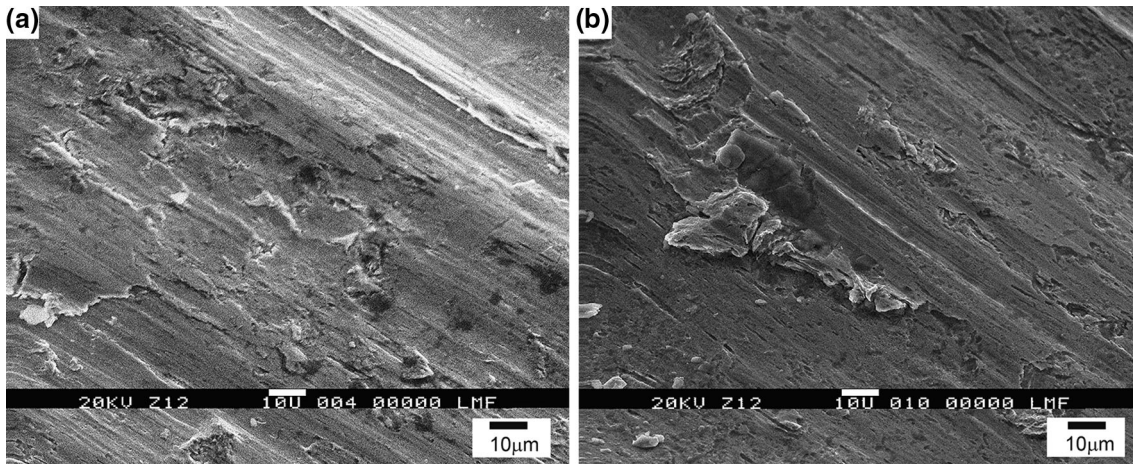

Fig. 11 Worn tracks for 15 N. (a) With lubricant, (b) without lubricant

prevents direct metal-to-metal contact (Ref 10, 26). Furthermore, induced martensite impedes adhesion leading also to lower COF. These facts can outweigh the load influence, leading to lower COF with 15 N than with 6 N (Fig. 7a). The load influence on weight loss percentages after friction tests is presented in Fig. 7(b). It turns out that as the load increases, the weight loss percentages increase in dry tests. In dry tests at 15 N, the effect of higher amount of hard martensite debris than at 6 N can cause higher wear, which enhances plowing (Ref 24). In addition to the described transfer lumps, grooves associated with the aforementioned mechanism are observed in Fig. 11(b). It is important to remark that no influence of the load on the COF nor on the weight loss percentages is observed in lubricated tests (Fig. 7a and b). These results are consistent with similar induced martensite percentages induced by the tribological tests performed at the different loads (Fig. 9b). Moreover, the observed stability and low COF are justified considering the reduction in the adhesion component due to the lubricant film. These results agree with the friction behavior reported in AISI 304 steel by Wei et al. (Ref 5) in similar test conditions.
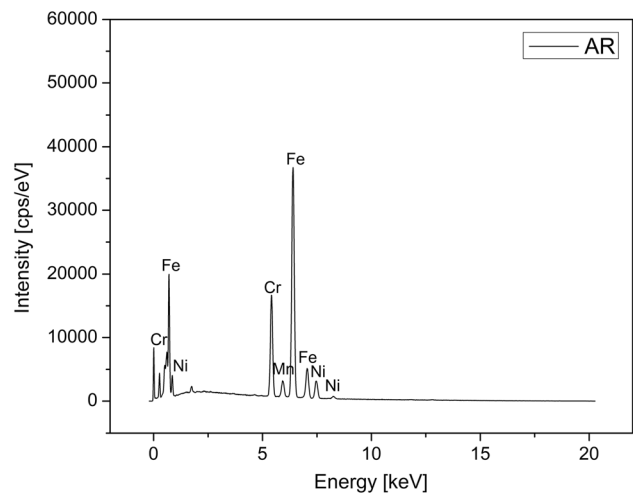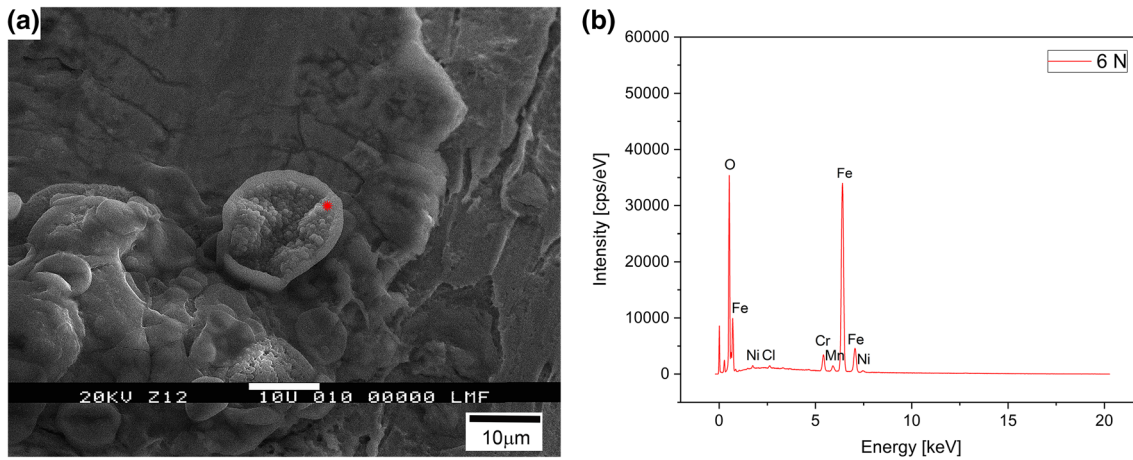

Fig. 12 EDS spectrum from the AR material

Fig. 13 Worn track without lubricant at 6 N. (a) SEM image, (b) EDS spectrum
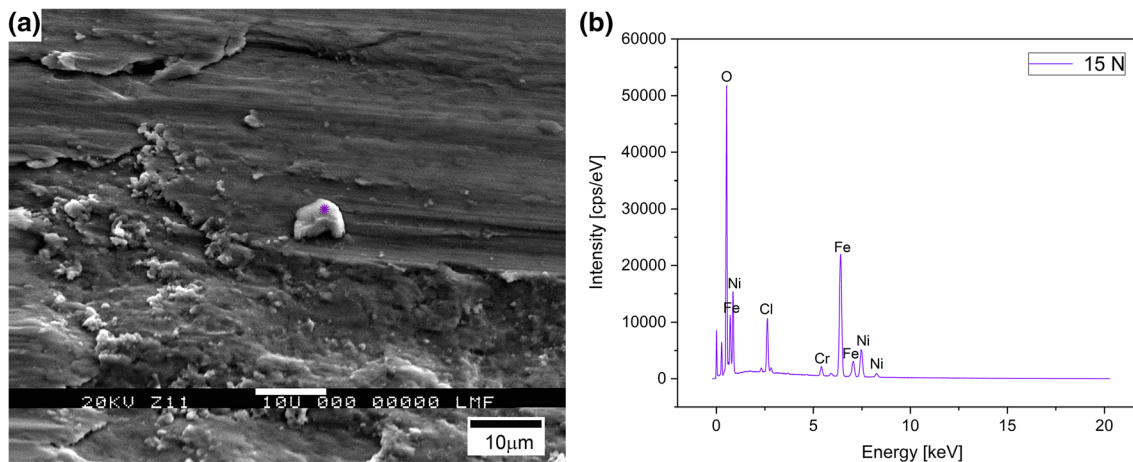

Fig. 14 Worn track without lubricant at 15 N. (a) SEM image, (b) EDS spectrum

4. Conclusions

The friction behavior analysis between a metastable stainless steel (AISI 304 L) and a 52100 steel ball using the ball-on-disc technique yields the following conclusions:

- Though the mechanical polishing produces an increase in the martensite volume fraction, work hardening dislocation structure and a decrease in roughness, no discernable effect on the friction behavior is observed. It seems that lower roughness can be outweighed by the higher induced hardness, leading to equivalent COF.
- Lubricant's role on the friction curves is determinant to achieve a lower and stable of COF.
- In dry tests, the increase in the applied load has no effect at the beginning of the COF behavior, but leads to a lower and more stable COF later. This effect can be explained by the difference in the amounts of induced martensite and oxidized particles. Higher wear losses are observed with increasing load due to harder martensite debris that enhances plowing.

References

1. M. Mcguire, Stainless Steels for Design Engineers. ASM Int., 2008. ISBN: 978-0-87170-717-8
2. K.H. Lo, C.H. Shek, and J.K.L. Lai, Recent Developments in Stainless Steels, *Mater. Sci. Eng. R*, 2009, **65**, p 39–104
3. M. Farias, R. Souza, A. Sinatora, and D. Tanaka, Influence of Applied Load, Sliding Velocity and Martensitic Transformation on the Unlubricated Sliding Wear of Austenitic Stainless Steels, *Wear*, 2007, **263**, p 773–781. https://doi.org/10.1016/j.wear.2006.12.017
4. J. Talonen. Effect of Strain-Induced α'-Martensite Transformation on Mechanical Properties of Metastable Austenitic Stainless Steels. Doctoral dissertation. Helsinki University of Technology Department of Mechanical Engineering Laboratory of Engineering Materials Helsinki, 2007
5. X. Wei, M. Hua, Z. Xue, Z. Gao, and J. Li, Evolution of Friction-Induced Microstructure of SUS 304 Meta-stable Austenitic Stainless

Steel and Its Influence on Wear Behavior, *Wear*, 2009, **267**, p 1386–1392. https://doi.org/10.1016/j.wear.2008.12.068

6. R. NafarDehsorkhi, S. Sabooni, F. Karimzadeh, A. Rezaeian, and M.H. Enayati, The Effect of Grain Size and Martensitic Transformation on the Wear Behavior of AISI, 304L Stainless Steel, *Mater. Des.*, 2014, **64**, p 56–62. https://doi.org/10.1016/j.matdes.2014.07.022

7. M. Zandrahimi, M. Reza Bateni, A. Poladi, and J.A. Szpunar, The Formation of Martensite During Wear of AISI, 304 Stainless Steel, *Wear*, 2007, **263**, p 674–678. https://doi.org/10.1016/j.wear.2007.01.107

8. G. Fargas, J.J. Roa, and A. Mateo, Influence of Pre-existing Martensite on the Wear Resistance of Metastable Austenitic Stainless Steels, *Wear*, 2016, **364-365**, p 40–47. https://doi.org/10.1016/j.wear.2016.06.018

9. W. Wang, M. Hua, and X. Wei, Friction Behavior of SUS 304 Metastable Austenitic Stainless Steel Sheet Against DC 53 Die Under the Condition of Friction Coupling Plastic Deformation, *Wear*, 2011, **271**, p 1166–1173. https://doi.org/10.1016/j.wear.2011.05.023

10. G. Chen, Y. Wei, S. Li, and W. Zhou, Friction and Wear Mechanism of Unlubricated 304L Austenitic Stainless Steel at Room Temperature, *J. Wuhan Univ. Technol. Mater.*, 2012, **27**, p 222–226. https://doi.org/10.1007/s11595-012-0441-3

11. M. Hua, X. Wei, and J. Li, Friction and Wear Behavior of SUS304 Austenitic Stainless Steel Against Al$_2$O$_3$ Ceramic Ball Under Relative High Load, *Wear*, 2008, **265**, p 799–810. https://doi.org/10.1016/j.wear.2008.01.017

12. D.M. Nuruzzaman and M.A. Chowdhury, *Friction Coefficient and Wear Rate of Different Materials Sliding*, J. Surf. Eng. Interdiscip. Mater. Sci, Int, 2013, https://doi.org/10.4018/ijseims.2013010103

13. Guía de acabados de Aceros Inoxidables, vol. 1, 2nd edn. Euro Inox, 2002. ISBN 2-87997-025-3

14. ISO 4288:2000, Geometrical Product Specifications (GPS), Surface Texture: Profile Method, Rules and Procedures for the Assessment of Surface Texture. International Organization for Standarization, 2000

15. ISO 3290-1:2014, Rolling Bearings—Balls—Part 1: Steel Balls. International Organization for Standarization, 2014

16. HertzWin 2.9.0. Vink System Design & Analysis (2009–2019). www.vinksda.com/toolkit-mechanical-calculations/hertz-contact-stress-calculations/. Accesed 23 May 2020

17. H.M. Rietveld, A profile refinement method for nuclear and magnetic structures, *J. Appl. Crystallogr.*, 1969, **2**, p 65–71. https://doi.org/10.1107/S0021889869006558

18. L. Lutterotti, S. Matthies, and H.-R. Wenk, Combined Texture and Structure Analysis of Deformed Limestone from Time-of-Flight Neutron Diffraction Spectra, *J. Appl. Phys.*, 1997, **81**, p 594–600. https://doi.org/10.1063/1.364220

19. L. Lutterotti. MAUD (Material Analysis Using Diffraction), 1997. http://maud.radiographema.com. Accesed 23 May 2020

20. J. Alves, L. Brandao, and A. Dos Santos Paula, The Influence of Sample Preparation on the Quantitative Analysis of the Volume Fraction of Martensite Formed in a 304L Trip Steel, *Mater. Res.*, 2015, **18**(Suppl 2), p 159–163

21. G. Straffelini, A Simplified Approach to the Adhesive Theory of Friction, *Wear*, 2001, **249**, p 79–85. https://doi.org/10.1016/S0043-1648(01)00524-5

22. P.L. Menezes and S.V. Kailas, Influence of Surface Texture and Roughness Parameters on Friction and Transfer Layer Formation During Sliding of Aluminium Pin on Steel Plate, *Wear*, 2009, **267**, p 1534–1549. https://doi.org/10.1016/j.wear.2009.06.003

23. R. Liu and D.Y. Li, Experimental Studies on Tribological Properties of PseudoelasticTiNi Alloy with Comparison to Stainless Steel 304, *Metall. Mater. Trans.*, 2000, **31A**, p 2773–2783

24. M. RezaBateni, J.A. Szpunar, X. Wang, and D.Y. Li, Wear and Corrosion Wear of Medium Carbon Steel and 304 Stainless Steel, *Wear*, 2006, **260**, p 116–122. https://doi.org/10.1016/j.wear.2004.12.037

25. G. Stachowiak, A. Batchelor. Engineering Tribology, 2nd edn. Butterworth Heinemann, London, 2000. ISBN:0750673044

26. G. Straffelini, D. Trabucco, and A. Molinari, Sliding Wear of Austenitic and Austenitic-Ferritic Stainless Steels, *Metall. Mater. Trans.*, 2002, **33A**, p 613–624. https://doi.org/10.1007/s11661-002-0123-4